PERGAMON

International Journal of Solids and Structures 40 (2003) 6389–6415

INTERNATIONAL JOURNAL OF SOLIDS and STRUCTURES

www.elsevier.com/locate/ijsolstr

Cracking of an orthotropic substrate reinforced by an orthotropic plate

R. Mahajan [a], F. Erdogan [b], B. Kilic [c], E. Madenci [c,*]

[a] *Assembly Technology Development, Intel Corporation, Chandler, AZ 85226, USA*

[b] *Department of Mechanical Engineering and Mechanics, Lehigh University, Bethlehem, PA 18015, USA*

[c] *Department of Aerospace and Mechanical Engineering, The University of Arizona, 1130 N. Mountain Avenue, Tucson, AZ 85721, USA*

Received 29 January 2003; received in revised form 11 July 2003

Abstract

A solution method is derived to determine the stress intensity factors for both an internal crack and an edge crack in an orthotropic substrate that is reinforced on its boundary by a finite-length orthotropic plate. The method utilizes the Green's functions for a pair of dislocations and a concentrated force on the boundary while invoking the concept of superposition. Enforcing the traction-free boundary condition along the crack surfaces and the continuity of displacement gradients along the plate/substrate interface results in a coupled system of singular integral equations. An asymptotic analysis of the kernels in these equations for the region of the junction point between the plate corner and the substrate boundary reveals the strength of the singularity in the case of an edge crack. The numerical solution of the integral equations provides results for the stress intensity factors for both an internal crack and an edge crack perpendicular to the substrate boundary and aligned with one of the corners of the plate. The present results have been validated against previously published stress intensity factors for an internal crack and an edge crack in an isotropic substrate.

Keywords: Crack; Substrate; Stress intensity factors; Thin film; Plate

1. Introduction

Relatively thin elastic layers bonded to elastic substrates, known as cover plates, reinforcements, coatings, and thin films, have a wide variety of engineering applications ranging from structural mechanics, thermal shielding and other forms of environmental protections to microelectronics. From the viewpoint of failure mechanics the questions of primary interest regarding these components are usually the accuracy of modeling and analysis of the likely failure processes. Thermally or mechanically induced loading failures that are often encountered in practice are cracking of the substrate at the edges of the reinforcement layer, de-bonding along the layer/substrate interface, and cracking of the layer.

* Corresponding author. Tel.: +1-520-621-6113; fax: +1-520-621-8191.
E-mail address: madenci@email.arizona.edu (E. Madenci).

0020-7683/$ - see front matter © 2003 Elsevier Ltd. All rights reserved.
doi:10.1016/S0020-7683(03)00421-9

Concerning microelectronics, the nature of the plate/substrate residual stresses was investigated by Hu (1979) and Isomae (1981, 1985), and the representation of these residual stresses in terms of far field stresses on the substrate was discussed by Erdogan and Joseph (1990). It is essential to investigate the stress field in order to analyze physical effects such as dislocation generation, film debonding and film and substrate distortion and cracking. Although the finite element analysis is capable of capturing the singular stress behavior near a corner or a crack tip in homogeneous regions with a refined mesh of conventional elements, it fails to capture the appropriate singular behavior near a corner or a crack tip at the junction of dissimilar materials.

Even without taking into account the possible inelastic and time-temperature effects, the actual three-dimensional problem of bonded layers of finite lengths for various crack geometries is analytically intractable. Depending on the relative dimensions of the adherents and the degree of accuracy required of the analysis, generally the problem is modeled under various approximating assumptions. The first set of assumptions, which are made largely for mathematical expediency, concerns the plane strain or axi-symmetry in loading and geometry and the piecewise homogeneity of the medium. The second set of assumptions concerns the mechanical behavior of the materials and usually requires that the adherents be linearly elastic, time-independent and isotropic, orthotropic, or anisotropic. The third group of assumptions involves certain simplifications regarding the distribution of the displacements or stresses in the non-homogeneous medium. If, for example, the thicknesses of the adherents are very small compared with the in-plane dimensions of the medium, then it may be possible to neglect all bending effects and model the adherents as "membranes" (Goodier and Hsu, 1954; Muki and Sternberg, 1968). The membrane model does, however, have a major drawback, in that it neglects the normal component of the load transfer along the interface, which is known to play an important role in the de-bonding process. Thus, despite relatively small adherent thicknesses, if the bending stiffness of the components is not negligible, a "plate" model may be employed for the adherents (Goland and Reissner, 1944; Delale et al., 1981). Other previous models treat the cover plate as a "membrane" and the substrate as an elastic continuum having finite (Erdogan and Civelek, 1974) or infinite thickness (Erdogan and Gupta, 1971a; Erdogan, 1971; Erdogan and Joseph, 1990) or assume both adherents to be elastic continua (Erdogan and Gupta, 1971b; Erdogan and Arin, 1972; Hutchinson and Suo, 1991). The emphasis in most of these studies was on de-bonding. The question of film fracture was briefly discussed by Erdogan and Joseph (1990). The problem of the substrate cracking at the edge of a membrane reinforcement was addressed by Delale and Erdogan (1982) for isotropic materials, and later by Mahajan et al. (1993) for orthotropic materials because Isomae (1981) reported that both the film and substrate demonstrate significant anisotropy in their elastic properties.

The previous work by Delale and Erdogan (1982) and Mahajan et al. (1993) employed a membrane model assuming that bending stiffness of the cover plate is negligible. This assumption concerns only the shear stresses while disregarding the normal stresses. Also, it removes the power singularity at the junction of plate/substrate junction. Furthermore, Erdogan and Joseph (1990) demonstrated that the stress singularity predicted by the membrane model can have a maximum difference of nearly 20 percent from the predictions of the more realistic plate model. Unlike the membrane model, the plate model with a bending stiffness captures the complex singular behavior of the coupled normal and shearing stresses. In the case of a membrane model, the shear stress has a square root singularity at the film edge. The magnitude of this stress intensity factor is dependent on a stiffness parameter that is a measure of the relative stiffnesses of the half-plane and the film. Delale and Erdogan (1982) concluded that the crack tends to propagate approximately normal to the half-plane surface. This conclusion is not entirely correct and the correct direction was determined by Erdogan and Joseph (1990) reporting that very near the film edge, the crack in the substrate tends to curve either towards the film or away from the film depending on the applied load on the film-substrate combination.

In this paper, the cracking of the substrate is considered by assuming that (i) the substrate is a semi-infinite orthotropic medium, (ii) the reinforcement is modeled as an orthotropic "plate," and (iii) the plane

of orthotropy perpendicular to the boundary is also the plane of weak fracture resistance in the substrate, and hence the crack starts at the end point of the plate reinforcement and propagates perpendicular to the boundary.

2. Problem statement

An orthotropic substrate having either an internal or an edge crack is reinforced by an orthotropic plate as described in Fig. 1. The substrate is semi-infinite in extent, and the plate has a thickness of h and a length of $2a$. The crack aligned with the right edge of the plate is perpendicular to the substrate boundary. In the case of an internal crack, the depth of the upper and lower crack tips from the boundary are denoted by c and d, leading to a crack length of $(d-c)$. In the case of an edge crack, the parameter c becomes zero. The crack surfaces are traction free and the plate/substrate interface is perfectly bonded.

The substrate is subjected to a uniform stress, σ_0, at infinity [i.e., $\sigma_{yy}(x,\pm\infty)=\sigma_0$] arising from a possible displacement mismatch along the plate/substrate interface (e.g. temperature changes) as suggested by Erdogan and Joseph (1990). The geometry of the medium and the applied loads are such that plane strain conditions prevail. A Cartesian coordinate system (x,y) is located at the junction of plate edge and

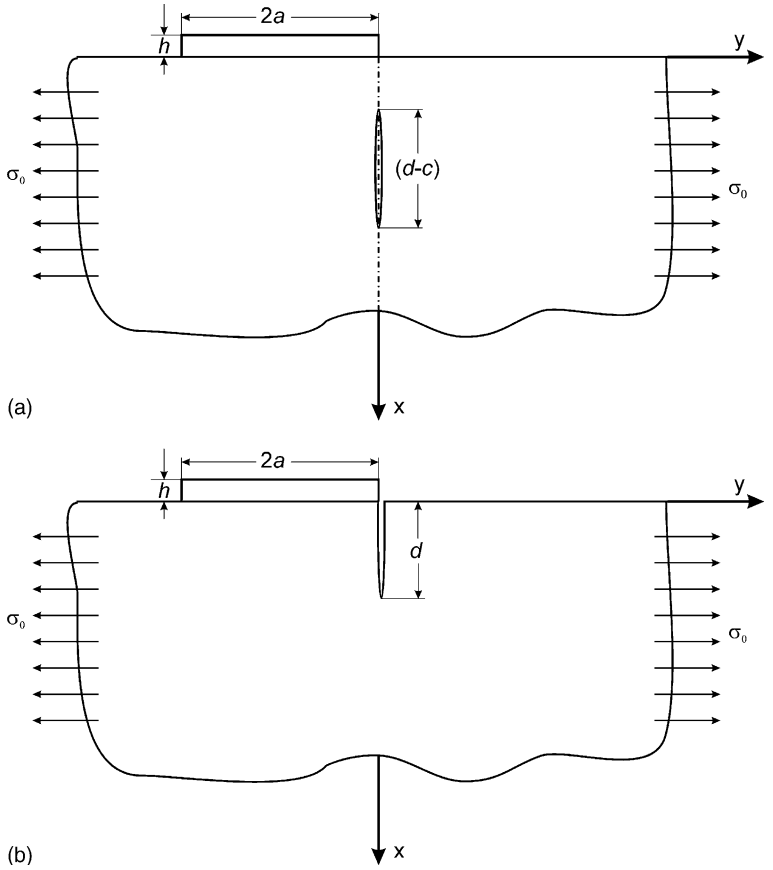

Fig. 1. Geometry of the orthotropic substrate reinforced by a plate containing an (a) internal crack and (b) edge crack.

boundary of the substrate. It coincides with the principal axes of orthotropy for both the substrate and plate. The relevant engineering material constants for the plate are specified by E_{yy}, G_{xy}, v_{yz}, and v_{zy}, and the substrate is characterized by stiffness coefficients, C_{ij}, with $(i,j=1,2,6)$. The displacement components in (x,y) directions in the plate and the substrate are denoted by (U,V) and (u,v), respectively. The stress components in the substrate are denoted by $\sigma_{\alpha\beta}$, with $\alpha,\beta=x,y$. The problem posed in this study is to determine the stress intensity factors associated with both the internal and edge cracks and the two corners of the reinforcement plate.

Although the solution of the resulting integral equations for the case of an internal crack is rather well-established, the physical assumptions concerning the edge crack lead to an integral equation of the 2nd kind with non-conjugate singularities, i.e., its index is not equal to 1, −1 or 0. The commonly employed techniques developed by Erdogan and his co-workers (1969, 1972 and 1973) and Theocaris and Ioakimides (1977) break down because of the presence of non-conjugate singularities at the edges. The specific contribution of this paper is the extraction of the non-conjugate singularities and the solution of the resulting coupled integral equations.

3. Formulation of the problem

Subjected to the conditions of traction-free crack surfaces and compatibility along the plate/substrate interface, the stress field and displacement gradients in the substrate with a crack can be composed of three loading conditions: (1) a dislocation at a point (x_1,y_1) in the substrate having a Burger's vector, **b** with components f_1 and f_2 parallel and perpendicular to the boundary, (2) a concentrated force acting at a point $(0,y_0)$ on the boundary of the substrate having components f_3 and f_4 parallel and perpendicular to the boundary, and (3) the applied load of $\sigma_{yy}(x,\pm\infty)=\sigma_0$ on the substrate. In view of the concept of superposition, the stress field and the displacement gradients in the substrate can be expressed in the form

$$\sigma_{xx}(x,y)=K_{11}f_1+K_{12}f_2+K_{13}f_3+K_{14}f_4, \tag{1a}$$

$$\sigma_{xy}(x,y)=K_{21}f_1+K_{22}f_2+K_{23}f_3+K_{24}f_4, \tag{1b}$$

$$\sigma_{yy}(x,y)=K_{31}f_1+K_{32}f_2+K_{33}f_3+K_{34}f_4+\sigma_0 \tag{1c}$$

and

$$\frac{\partial}{\partial y}u(x,y)=M_{11}f_1+M_{12}f_2+M_{13}f_3+M_{14}f_4, \tag{2a}$$

$$\frac{\partial}{\partial y}v(x,y)=M_{21}f_1+M_{22}f_2+M_{23}f_3+M_{24}f_4+\beta_{22}\sigma_0, \tag{2b}$$

where f_1, f_2, f_3, and f_4 are unknown distributed functions and K_{ij} and M_{ij} are the Green's functions, whose explicit forms are given in Appendix A. The term $\beta_{22}\sigma_0$ represents the displacement gradient arising from the loading of $\sigma_{yy}(x,\pm\infty)=\sigma_0$ on the substrate in the absence of a crack, and the compliance coefficient $\beta_{22}=C_{11}/(C_{11}C_{22}-C_{12}^2)$.

Traction-free crack surfaces are enforced by requiring that

$$\sigma_{yy}(x,\pm 0)=0, \quad c<x<d, \tag{3a}$$

$$\sigma_{xy}(x,\pm 0)=0, \quad c<x<d. \tag{3b}$$

The compatibility conditions along the plate/substrate interface are satisfied by requiring that

$$\frac{\partial}{\partial y}u(0,y) = \frac{\partial}{\partial y}U(y), \quad -2a < y < 0, \tag{4a}$$

$$\frac{\partial}{\partial y}v(0,y) = \frac{\partial}{\partial y}V(h/2,y), \quad -2a < y < 0, \tag{4b}$$

where the explicit form of the displacement gradients in the plate in terms of the unknown functions f_3, and f_4 are derived in Appendix B.

The dislocation densities f_1 and f_2 are related to the crack surface displacements by

$$f_1(x) = -\frac{\partial}{\partial x}[v(x,+0) - v(x,-0)], \tag{5a}$$

$$f_2(x) = -\frac{\partial}{\partial x}[u(x,+0) - u(x,-0)]. \tag{5b}$$

Therefore, in the case of an internal crack, the single-valuedness condition of displacements requires that

$$\int_c^d f_1(t)\,\mathrm{d}t = 0, \tag{6a}$$

$$\int_c^d f_2(t)\,\mathrm{d}t = 0. \tag{6b}$$

However, these constraint conditions are not applicable in the case of an edge crack.

The surface tractions acting on the reinforcement plate (shear and normal stresses along the interface between the plate and substrate) are defined as

$$\sigma_{xy}(0,y_0) = f_3(y_0), \quad \sigma_{xx}(0,y_0) = f_4(y_0), \qquad -2a < y_0 < 0 \tag{7}$$

and they must satisfy the force and moment equilibrium conditions leading to

$$\int_{-2a}^0 f_3(y_0)\,\mathrm{d}y_0 = 0, \tag{8a}$$

$$\int_{-2a}^0 f_4(y_0)\,\mathrm{d}y_0 = 0, \tag{8b}$$

$$\int_{-2a}^0 y_0 f_4(y_0)\,\mathrm{d}y_0 = 0. \tag{8c}$$

3.1. Internal crack

Having a continuous distribution of dislocation, $\mathbf{b} = \langle f_1, f_2\rangle$, along the crack surfaces, i.e., $x_1 = t$ and $y_1 = 0$ for $c < t < d$, and enforcing the boundary and compatibility conditions, Eqs. (3) and (4), result in the following system of singular integral equations:

$$\frac{1}{\pi}\int_c^d \frac{f_1(t)}{t-x}\,\mathrm{d}t + \int_c^d N_{11}(x,t)f_1(t)\,\mathrm{d}t + \int_c^d N_{12}(x,t)f_2(t)\,\mathrm{d}t + \int_{-2a}^0 N_{13}(x,y_0)f_3(y_0)\,\mathrm{d}y_0 + \int_{-2a}^0 N_{14}(x,y_0)f_4(y_0)\,\mathrm{d}y_0 = \frac{2\sigma_0}{K_n} \quad (c<x<d), \tag{9a}$$

$$\frac{1}{\pi}\int_c^d \frac{f_2(t)}{t-x}\,\mathrm{d}t + \int_c^d N_{21}(x,t)f_1(t)\,\mathrm{d}t + \int_c^d N_{22}(x,t)f_2(t)\,\mathrm{d}t + \int_{-2a}^0 N_{23}(x,y_0)f_3(y_0)\,\mathrm{d}y_0 + \int_{-2a}^0 N_{24}(x,y_0)f_4(y_0)\,\mathrm{d}y_0 = 0 \quad (c<x<d), \tag{9b}$$

$$\frac{1}{\pi}\int_{-2a}^0 \frac{f_3(y_0)}{y_0-y}\,\mathrm{d}y_0 - \frac{S_1}{S_2}f_4(y) + \int_c^d N_{31}(y,t)f_1(t)\,\mathrm{d}t + \int_c^d N_{32}(y,t)f_2(t)\,\mathrm{d}t + \int_{-2a}^0 N_{33}(y,y_0)f_3(y_0)\,\mathrm{d}y_0 + \int_{-2a}^0 N_{34}(y,y_0)f_4(y_0)\,\mathrm{d}y_0 = \frac{\beta_{22}\sigma_0}{S_2} \quad (-2a<y<0), \tag{9c}$$

$$\frac{1}{\pi}\int_{-2a}^0 \frac{f_4(y_0)}{y_0-y}\,\mathrm{d}y_0 + \frac{R_1}{R_2}f_3(y) + \int_c^d N_{41}(y,t)f_1(t)\,\mathrm{d}t + \int_c^d N_{42}(y,t)f_2(t)\,\mathrm{d}t + \int_{-2a}^0 N_{43}(y,y_0)f_3(y_0)\,\mathrm{d}y_0 + \int_{-2a}^0 N_{44}(y,y_0)f_4(y_0)\,\mathrm{d}y_0 = -\frac{\psi_y(-2a)}{R_2} \quad (-2a<y<0), \tag{9d}$$

where the parameters and the kernels are given in Appendix A. The last two of these integral equations, Eqs. (9c) and (9d) are of the second kind and can be combined as follows by multiplying Eq. (9d) by $-\mathrm{i}\eta$ and adding to (9c) while invoking $R_1 = S_1$

$$\frac{1}{\mathrm{i}\pi}\int_{-2a}^0 \frac{\phi(y_0)}{y_0-y}\,\mathrm{d}y_0 - \gamma\phi(y) + \int_c^d M_1(y,t)f_1(t)\,\mathrm{d}t + \int_c^d M_2(y,t)f_2(t)\,\mathrm{d}t + \int_{-2a}^0 M_3(y,y_0)\phi(y_0)\,\mathrm{d}y_0 + \int_{-2a}^0 M_4(y,y_0)\phi^*(y_0)\,\mathrm{d}y_0 = \frac{\beta_{22}\sigma_0}{S_2} + \mathrm{i}\eta\frac{\psi_y(-2a)}{R_2} \quad (-2a<y<0), \tag{10}$$

where the auxiliary function, $\phi(y)$, having $\phi^*(y)$ as its complex conjugate is defined as

$$\phi(y) = \eta f_4(y) + \mathrm{i}f_3(y), \tag{11}$$

with $\eta = \sqrt{R_2/S_2}$ and $\gamma = R_1/\sqrt{R_2S_2}$. The known kernels, $M_i(y,t)$, are defined in Appendix A. The solution to the system of singular integral equations given by Eqs. (9a), (9b), and (10) permits the determination of f_1, f_2, f_3, f_4, and $\psi_y(-2a)$ subject to the five constraint conditions given in Eqs. (6) and (8). The moment equilibrium condition (8c) accounts for the unknown rotation, $\psi_y(-2a)$.

In the integral equations, Eqs. (9a) and (9b), the dominant parts of the kernels have only a Cauchy-type singularity and, therefore, for $c > 0$, the solutions to $f_1(x)$ and $f_2(x)$ have the form

$$\frac{K_n}{2}f_1(x) = \frac{\Phi_1(x)}{(x-c)^{\beta_1}(d-c)^{\alpha_1}}, \tag{12a}$$

$$\frac{K_e}{2}f_2(x) = \frac{\Phi_2(x)}{(x-c)^{\beta_2}(d-c)^{\alpha_2}}, \tag{12b}$$

where $\alpha_1 = \alpha_2 = \beta_1 = \beta_2 = 1/2$ and Φ_1 and Φ_2 are unknown bounded functions. The constants K_n and K_e involving material stiffness coefficients, C_{ij}, are given in Appendix A. As suggested by Muskhelishvili (1953), the solution to the dominant part of the integral equation of the second kind, Eq. (10), is of the form

$$\phi(y) = \frac{\Phi_3(y)}{(y+2a)^{\alpha_3}(-y)^{\beta_3}}, \tag{13a}$$

with

$$\alpha_3 = \frac{1}{2} + \mathrm{i}\omega, \quad \beta_3 = \frac{1}{2} - \mathrm{i}\omega, \qquad \text{with } \omega = \frac{1}{2\pi}\ln\left(\frac{1-\gamma}{1+\gamma}\right) \tag{13b}$$

and $\Phi_3(y)$ is an unknown bounded function.

3.2. Edge crack

The integral equations given in Eqs. (9a), (9b), and (10) are also valid in the case of an edge crack for which $c = 0$ with the requirement that the junction of plate edge and substrate at the point $(x = 0, y = 0)$ has a common point of singularity for the unknown functions f_1, f_2, and ϕ. In view of Eqs. (12) and (13), the solution forms for the unknown functions f_1, f_2, and ϕ having a common singularity at $(x = 0, y = 0)$ can be written as

$$f_1(t) = \frac{\Phi_1(t)}{t^{\beta}(d-t)^{\alpha_1}}, \quad 0 < t < d, \tag{14a}$$

$$f_2(t) = \frac{\Phi_2(t)}{t^{\beta}(d-t)^{\alpha_2}}, \quad 0 < t < d, \tag{14b}$$

$$\phi(y_0) = \frac{\Phi_3(y_0)}{(-y_0)^{\beta}(y_0+2a)^{\alpha_3}}, \quad -2a < y_0 < 0. \tag{14c}$$

However, the kernels N_{ij}, which are bounded in the closed intervals $[c, d]$ and $[-2a, 0]$ for $c > 0$, become unbounded when the pairs of variables (x, t), (x, y_0), and (y, t) approach the junction point of $(x = 0, y = 0)$ simultaneously. Furthermore for $c = 0$, the kernels of the integral equations are of the generalized Cauchy-type. For example, by separating into partial fractions, the kernel N_{11} may be expressed as

$$\pi C_h N_{11}(x,t) = \frac{p+2}{t+x} - \frac{2(2+pp_1)}{(p_1-p_2)(t-p_1x)} + \frac{2(2+pp_2)}{(p_1-p_2)(t-p_2x)}, \quad 0 < (t,x) < d, \tag{15}$$

where $(p_1, p_2) = -p \mp \sqrt{p^2-4}/2$ with $p = C_h + 2$ and $-4 < C_h < \infty$. The integral appearing in Eq. (9a) can then be expressed as

$$\int_0^d N_{11}(x,t) f_1(t)\,\mathrm{d}t = \frac{1}{C_h}\sum_{j=1}^{3}\frac{A_j}{\pi}\int_0^d \frac{f_1(t)}{t-z_j}\,\mathrm{d}t, \quad 0 < x < d. \tag{16}$$

The variables p_1 and p_2 are complex conjugates of each other for $-4 < C_h < 0$, and real and negative for $C_h \geqslant 0$, meaning that for $0 < x < d$, the variables z_j are outside the cut $[0, d]$ as shown in Fig. 5. In their polar form, these variables are defined as $z_j = r_j x \mathrm{e}^{\mathrm{i}\theta_j}$, with $\theta_j = \pi$ for $j = 1, 2, 3$, $r_1 = 1$, $r_2 = |p_1|$, and $r_3 = |p_2|$ for $C_h \geqslant 0$. For $-4 < C_h < 0$, the definitions of θ_2 and θ_3 become $\theta_2 = \mathrm{Arg}(p_1)$ and $\theta_3 = \mathrm{Arg}(p_2)$.

The kernel N_{11} becomes unbounded as t and z_j approach zero simultaneously. Such unbounded kernels influence the nature of the singularity at the point of $(x = 0, y = 0)$. The strength of this singularity can be determined by utilizing the asymptotic expressions for a sectionally holomorphic function given by Muskhelishvili (1953). The explicit expression for these asymptotic expressions are given in Appendix C. Based on these expressions, the integral given in Eq. (16) can be rewritten in the form

$$\int_0^d N_{11}(x,t)f_1(t)\,\mathrm{d}t = \frac{1}{C_h}\sum_{j=1}^{3} A_j \frac{\Phi_1(0)}{d^{\alpha_1}} \frac{\mathrm{e}^{\mathrm{i}(\pi-\theta_j)\beta}}{\sin\pi\beta} \frac{1}{(r_j x)^{\beta}} + h(x). \tag{17}$$

Similarly, the dominant part of this singular integral equation, Eq. (9a), can be expressed as

$$\frac{1}{\pi}\int_0^d \frac{f_1(t)}{t-x}\,\mathrm{d}t = \frac{\Phi_1(0)}{d^{\alpha_1}}\frac{\cot\pi\beta}{x^{\beta}} - \frac{\Phi_1(d)}{d^{\beta}}\frac{\cot\pi\alpha_1}{(d-x)^{\alpha_1}} + G_0(z). \tag{18}$$

All of the singular terms in the integral equations in Eqs. (9a), (9b), and (10), including those coming from the generalized Cauchy kernels, such as that given by Eq. (16), can be obtained by using the asymptotic relations. These integral equations can then be expressed in the form

$$\sum_{k=1}^{8} B_{jk}(\beta,\alpha_1,\alpha_2,\alpha_3)D_k(x_0) + H_j(x_0) = 0, \quad j = 1,2,3,4, \tag{19}$$

where $x_0 = x$ or $x_0 = -y$, B_{jk} are known bounded functions, and H_j represent all bounded and lower order singular terms. The unknown functions D_k are defined as

$$(D_1,\ldots,D_8) = \left(\frac{\Phi_1(0)}{d^{\alpha_1}x^{\beta}}, \frac{\Phi_1(d)}{d^{\beta}(d-x)^{\alpha_1}}, \frac{\Phi_2(0)}{d^{\alpha_2}x^{\beta}}, \frac{\Phi_2(d)}{d^{\beta}(d-x)^{\alpha_2}}, \frac{\mathrm{Re}[\Phi_3(0)]}{(2a)^{\alpha_3}(-y)^{\beta}}, \frac{\mathrm{Im}[\Phi_3(0)]}{(2a)^{\alpha_3}(-y)^{\beta}}, \frac{\mathrm{Re}[\Phi_3(d)]}{(2a)^{\beta}(2a+y)^{\alpha_3}}, \frac{\mathrm{Im}[\Phi_3(d)]}{(2a)^{\beta}(2a+y)^{\alpha_3}}\right) \tag{20}$$

in which the functions Φ_j are non-zero at the end points 0, d and $-2a$. Thus, multiplying Eq. (18) by $(d-x)^{\alpha_1}$, $(d-x)^{\alpha_2}$, and $(2a+y)^{\alpha_3}$ and letting x approach d and y approach $-2a$, respectively, results in

$$\cot\pi\alpha_1 = 0, \tag{21a}$$

$$\cot\pi\alpha_2 = 0, \tag{21b}$$

$$\cot^2\pi\alpha_3 + \gamma^2 = 0 \tag{21c}$$

whose solutions lead to

$$\alpha_1 = \alpha_2 = \frac{1}{2}, \quad \alpha_3 = \frac{1}{2} + \mathrm{i}\omega, \quad \omega = \frac{1}{2\pi}\ln\left(\frac{1-\gamma}{1+\gamma}\right). \tag{22}$$

Similarly, multiplying Eq. (18) by x^{β} or y^{β} and letting both x and y approach zero results in

$$\sum_{j=1}^{4} R_{ij}(\beta)L_i = 0, \quad i = 1,2,3,4 \tag{23}$$

in which R_{ij} are known functions and L_j represent the unknown non-zero coefficients defined by

$$(L_1,L_2,L_3,L_4) = \left(\frac{\Phi_1(0)}{d^{\alpha_1}}, \frac{\Phi_2(0)}{d^{\alpha_2}}, \frac{\mathrm{Re}[\Phi_3(0)]}{(2a)^{\alpha_3}}, \frac{\mathrm{Im}[\Phi_3(0)]}{(2a)^{\alpha_3}}\right). \tag{24}$$

For example, the expression for $R_{11}(\beta)$ is obtained from the limiting values of Eqs. (17) and (18) as

$$R_{11}(\beta) \sim \lim_{x\to 0} x^{\beta}\left\{\int_0^d N_{11}(x,t)f_1(t)\,\mathrm{d}t + \frac{1}{\pi}\int_0^d \frac{f_1(t)}{t-x}\,\mathrm{d}t\right\} = \left\{\sum_{j=1}^{3}\frac{A_j\mathrm{e}^{\mathrm{i}(\pi-\theta_j)\beta}}{C_h\sin\pi\beta r_i^{\beta}} + \cot\pi\beta\right\}\frac{\Phi_1(0)}{d^{\alpha_1}} \tag{25}$$

leading to

$$R_{11}(\beta) = \cot \pi\beta + \sum_{j=1}^{3} \frac{A_j e^{i(\pi-\theta_j)\beta}}{C_h \sin \pi\beta}. \tag{26}$$

The coefficients A_j are all real for $C_h \geqslant 0$, and only A_2 and A_3 are complex conjugates of each other for $-4 < C_h < 0$, resulting in real values for $R_{11}(\beta)$.

Requiring the determinant of the coefficient matrix of the homogeneous system of equations, Eq. (23), to vanish leads to the determination of the strength of the singularity, β. Unlike the bounded stress state at the singular point of a membrane reinforcement considered by Delale and Erdogan (1982) and Mahajan et al. (1993), the characteristic equation, Eq. (23), associated with the plate reinforcement, always has a root in the strip $0 < \mathrm{Re}[\beta] < 1$, which is real and less than one-half. It should be pointed out that if one considers the symmetric problem for two identical reinforcements along $-2a < y < 0$ and $0 < y < 2a$, f_2 would be zero; and instead of Eq. (23), a system of three algebraic equations would exist, leading to a simpler characteristic equation. Despite this, the physics of the problem requires that the value of β to be the same for both cases. Indeed, this problem was formulated, and it was observed that the two characteristic equations lead to identical results for β. Details of the asymptotic analysis giving the characteristic equations for edge crack problems in isotropic and orthotropic half planes reinforced by a single or two symmetrical plates were given by Mahajan (1991). For a specific value of β rendering the characteristic equation, Eq. (23) to be zero, the system of equations provides three linearly independent equations in the form

$$\sum_{j=1}^{3} S_{ij}(\beta) L_i = 0, \quad i = 1, 2, 3. \tag{27}$$

These three equations serve as constraint conditions in the solution of the singular integral equations, Eqs. (9a), (9b), and (10), with $c = 0$.

It is worth noting that the results of β found herein from the asymptotic analysis of a "plate" bonded to a 90-degree elastic wedge, formed where the crack edge meets the plate edge, agree exactly with the continuum elasticity results obtained for two 90-degree wedges where one of the wedges is perfectly rigid. This was verified by comparing results for the isotropic case in the present analysis with the results reported by Bogy (1970). It is in the nature of the plate model adopted in this study that β is completely independent of the elastic properties of the plate. Because $\gamma = R_1/\sqrt{R_2 S_2}$ is dependent on the elastic constants of the substrate only, as observed in Eqs. (13b) and (22), the nature of the singularity at the other end of the plate $y = -2a$, which does not involve the edge crack intersecting the surface, is also independent of the elastic properties of the plate.

4. Solution of the integral equations

Prior to the numerical solution of the coupled integral equations, Eqs. (9a), (9b), and (10), they are normalized by introducing

$$x = \frac{d-c}{2} r + \frac{d+c}{2}, \quad t = \frac{d-c}{2} r_0 + \frac{d+c}{2}, \quad -1 < (r, r_0) < 1, \tag{28a}$$

$$y = a(s-1), \quad y_0 = a(s_0 - 1), \quad -1 < (s, s_0) < 1 \tag{28b}$$

leading to

$$\frac{P_1}{\pi}\int_{-1}^{1}\frac{g_1(r_0)}{r_0-r}\,\mathrm{d}r_0+\int_{-1}^{1}H_{11}(r,r_0)g_1(r_0)\,\mathrm{d}r_0+\int_{-1}^{1}H_{12}(r,r_0)g_2(r_0)\,\mathrm{d}r_0+\int_{-1}^{1}H_{13}(r,s_0)g_3(s_0)\,\mathrm{d}s_0+\int_{-1}^{1}H_{14}(r,s_0)g_3^*(s_0)\,\mathrm{d}s_0=q_1(r)=\frac{2\sigma_0}{K_n},\tag{29a}$$

$$\frac{P_2}{\pi}\int_{-1}^{1}\frac{g_2(r_0)}{r_0-r}\,\mathrm{d}r_0+\int_{-1}^{1}H_{21}(r,r_0)g_1(r_0)dr_0+\int_{-1}^{1}H_{22}(r,r_0)g_2(r_0)\,\mathrm{d}r_0+\int_{-1}^{1}H_{23}(r,s_0)g_3(s_0)\,\mathrm{d}s_0+\int_{-1}^{1}H_{24}(r,s_0)g_3^*(s_0)\,\mathrm{d}s_0=q_2(r)=0,\tag{29b}$$

$$\frac{P_3}{\pi}\int_{-1}^{1}\frac{g_3(s_0)}{s_0-s}\,\mathrm{d}s_0+R_3g_3(s)+\int_{-1}^{1}H_{31}(s,r_0)g_1(r_0)\,\mathrm{d}r_0+\int_{-1}^{1}H_{32}(s,r_0),g_2(r_0)\,\mathrm{d}r_0+\int_{-1}^{1}H_{33}(s,s_0)g_3(s_0)\,\mathrm{d}s_0+\int_{-1}^{1}H_{34}(s,s_0)g_3^*(s_0)\,\mathrm{d}s_0=q_3(s)=\frac{\beta_{22}\sigma_0}{S_2}+\mathrm{i}\eta\frac{\psi_y(-2a)}{R_2}\tag{29c}$$

in which g_1, g_2, and g_3 with its complex conjugate g_3^* are the unknown functions and $\psi_y(-2a)$ is an unknown constant. The definition of the parameters P_i and the kernels H_{ij} are given in Appendix A. In the case of an internal crack, the constraint conditions of Eqs. (6) and (8) are rewritten as

$$\int_{-1}^{1}g_1(r_0)\,\mathrm{d}r_0=0,\quad\int_{-1}^{1}g_2(r_0)\,\mathrm{d}r_0=0,\tag{30a,b}$$

$$\int_{-1}^{1}[g_3(s_0)-g_3^*(s_0)]\,\mathrm{d}s_0=0,\quad\int_{-1}^{1}[g_3(s_0)+g_3^*(s_0)]\,\mathrm{d}s_0=0,\quad\int_{-1}^{1}(s_0-1)[g_3(s_0)+g_3^*(s_0)]\,\mathrm{d}s_0=0.\tag{30c,d,e}$$

In the case of an edge crack, the first two constraint conditions, Eqs. (30a) and (30b), enforcing single-valuedness are no longer valid. However, they are replaced with the three conditions arising from the asymptotic analysis, Eq. (27). Invoking the normalization parameters given in Eq. (28), these constraint conditions are rewritten as

$$\begin{aligned}&h_{11}(\beta)G_1(-1)+h_{12}(\beta)G_2(-1)+h_{13}(\beta)G_3(1)+h_{14}(\beta)G_3^*(1)=0,\\&h_{21}(\beta)G_1(-1)+h_{22}(\beta)G_2(-1)+h_{23}(\beta)G_3(1)+h_{24}(\beta)G_3^*(1)=0,\\&h_{31}(\beta)G_1(-1)+h_{32}(\beta)G_2(-1)+h_{33}(\beta)G_3(1)+h_{34}(\beta)G_3^*(1)=0\end{aligned}\tag{31}$$

in which h_{ij} are expressed in terms of S_{ij}.

The unknown functions, f_1, f_2, and ϕ whose solution forms are given by Eqs. (12) and (13) are rewritten in terms of the normalized variables as

$$\frac{K_n}{2}f_1(x)\equiv g_1(r)=\frac{G_1(r)}{(1-r)^{\alpha_1}(1+r)^{\beta_1}},\tag{32a}$$

$$\frac{K_e}{2}f_2(x)\equiv g_2(r)=\frac{G_2(r)}{(1-r)^{\alpha_2}(1+r)^{\beta_2}},\tag{32b}$$

$$\phi(y)\equiv g_3(s)=\frac{G_3(s)}{(1-s)^{\beta_3}(1+s)^{\alpha_3}}\tag{32c}$$

for the internal crack and as

$$\frac{K_n}{2} f_1(x) \equiv g_1(r) = \frac{G_1(r)}{(1-r)^{\alpha_1}(1+r)^{\beta}}, \tag{33a}$$

$$\frac{K_e}{2} f_2(x) \equiv g_2(r) = \frac{G_2(r)}{(1-r)^{\alpha_2}(1+r)^{\beta}}, \tag{33b}$$

$$\phi(y) \equiv g_3(s) = \frac{G_3(s)}{(1-s)^{\beta}(1+s)^{\alpha_3}} \tag{33c}$$

for the edge crack. The unknown auxiliary functions, $G_1(r)$, $G_2(r)$, and $G_3(s)$ permit the evaluation of the singular stresses around the crack tips and at the end points of the reinforcement plate. For the internal crack, the stress intensity factors representing the singularities are defined as (Mahajan et al., 1993)

$$k_1(d) = \lim_{x\to d} 2^{\beta_1}(x-d)^{\alpha_1}\sigma_{yy}(x,0) = \lim_{x\to d} 2^{\beta_1}(d-x)^{\alpha_1}\frac{K_n}{2} f_1(x) = G_1(1)\left(\frac{d-c}{2}\right)^{\alpha_1}, \tag{34a}$$

$$k_2(d) = \lim_{x\to d} 2^{\beta_2}(x-d)^{\alpha_2}\sigma_{xy}(x,0) = \lim_{x\to d} 2^{\beta_2}(d-x)^{\alpha_2}\frac{K_e}{2} f_2(x) = G_2(1)\left(\frac{d-c}{2}\right)^{\alpha_2}, \tag{34b}$$

$$k_1(c) = \lim_{x\to c} 2^{\alpha_1}(c-x)^{\beta_1}\sigma_{yy}(x,0) = -\lim_{x\to c} 2^{\alpha_1}(x-c)^{\beta_1}\frac{K_n}{2} f_1(x) = -G_1(-1)\left(\frac{d-c}{2}\right)^{\beta_1}, \tag{34c}$$

$$k_2(c) = \lim_{x\to c} 2^{\alpha_2}(c-x)^{\beta_2}\sigma_{xy}(x,0) = -\lim_{x\to c} 2^{\alpha_2}(x-c)^{\beta_2}\frac{K_e}{2} f_2(x) = -G_2(-1)\left(\frac{d-c}{2}\right)^{\beta_2}, \tag{34d}$$

$$k(0) = \eta k_1(0) + \mathrm{i}k_2(0) = \lim_{y\to 0} 2^{\alpha_3}(-y)^{\beta_3}[\eta\sigma_{xx}(0,y) + \mathrm{i}\sigma_{xy}(0,y)] = G_3(1)a^{\beta_3}, \tag{34e}$$

$$k(-2a) = \eta k_1(-2a) + \mathrm{i}k_2(-2a) = \lim_{y\to -2a} 2^{\beta_3}(y+2a)^{\alpha_3}[\eta\sigma_{xx}(0,y) + \mathrm{i}\sigma_{xy}(0,y)] = G_3(-1)a^{\alpha_3}. \tag{34f}$$

Similarly, for the edge crack they are defined as

$$k_1(d) = \lim_{x\to d} 2^{\beta}(x-d)^{\alpha_1}\sigma_{yy}(x,0) = \lim_{x\to d} 2^{\beta}(d-x)^{\alpha_1}\frac{K_n}{2} f_1(x) = G_1(1)\left(\frac{d-c}{2}\right)^{\alpha_1}, \tag{35a}$$

$$k_2(d) = \lim_{x\to d} 2^{\beta}(x-d)^{\alpha_2}\sigma_{xy}(x,0) = \lim_{x\to d} 2^{\beta}(d-x)^{\alpha_2}\frac{K_e}{2} f_2(x) = G_2(1)\left(\frac{d-c}{2}\right)^{\alpha_2}, \tag{35b}$$

$$k(0) = \eta k_1(0) + \mathrm{i}k_2(0) = \lim_{y\to 0} 2^{\alpha_3}(-y)^{\beta}[\eta\sigma_{xx}(0,y) + \mathrm{i}\sigma_{xy}(0,y)] = G_3(1)a^{\beta}, \tag{35c}$$

$$k(-2a) = \eta k_1(-2a) + \mathrm{i}k_2(-2a) = \lim_{y\to -2a} 2^{\beta}(y+2a)^{\alpha_3}[\eta\sigma_{xx}(0,y) + \mathrm{i}\sigma_{xy}(0,y)] = G_3(-1)a^{\alpha_3}. \tag{35d}$$

By computing the crack closure energy, in the orthotropic region under consideration, the strain energy release at a given crack tip may be obtained as

$$\mathscr{G} = \frac{\pi}{2}\left(\frac{k_1^2}{K_n} + \frac{k_2^2}{K_e}\right). \tag{36}$$

The complexity of the kernels in Eqs. (9a), (9b), and (10) requires that the singular integral equation be solved numerically. The procedure involves the reduction of the integral equations and constraints to a system of algebraic equations using the collocation technique introduced by Miller and Keer (1985) and later extended by Quan (1991) to include the generalized Cauchy kernel, and by Kabir et al. (1998) to consider integral equations with logarithmic-, Cauchy-, and Hadamard-type singularities. In this technique, the quadrature interval $[-1,1]$ is partitioned into a series of subintervals over which the unknown functions, G_i, with $i=1,2,3$, are approximated by quadratic Lagrange interpolation polynomials. The integration points, r_{0i} or s_{0i}, are at the ends and at the midpoint of each subinterval obtained by dividing the interval $[-1,1]$ into N_i subintervals associated with each G_i. The collocation points, r_j or s_j, are defined at the midpoint of two consecutive integration points, i.e., $r_j=(r_{0j}+r_{0(j+1)})/2$ or $s_j=(s_{0j}+s_{0(j+1)})/2$, with $j=1,2,\ldots,2N_i$. Thus, the unknown functions are approximated over each subinterval k $(t_{2k-1}\leqslant t\leqslant t_{2k+1})$ by

$$G_i(t)\approx G_{i(2k-1)}[(t-t_{2k})^2/2h_k^2-(t-t_{2k})/2h_k]+G_{i(2k)}[1-(t-t_{2k})^2/h_k^2]+G_{i(2k+1)}[(t-t_{2k})^2/2h_k^2 + (t-t_{2k})/2h_k], \tag{37}$$

where $G_{i(k)}=G_i(t_k)$, with $i=1,2,3$, and $h_k=(t_{2k+1}-t_{2k-1})/2$, with t representing either r_0 or s_0. As a result of this discretization, Eqs. (29), (30), and (31) can be written as

$$\frac{P_1}{\pi}\sum_{i=1}^{2N_1+1} w_{1i}(r_j)G_{1(i)}+\sum_{i=1}^{2N_1+1} H_{11}(r_j,r_{0i})v_{1i}G_{1(i)}+\sum_{i=1}^{2N_2+1} H_{12}(r_j,r_{0i})v_{2i}G_{2(i)}+\sum_{i=1}^{2N_3+1} H_{13}(r_j,s_{0i})v_{3i}G_{3(i)} + \sum_{i=1}^{2N_3+1} H_{14}(r_j,s_{0i})v_{3i}^*G_{3(i)}^*=q_1(r_j),\quad j=1,\ldots,2N_1, \tag{38a}$$

$$\frac{P_2}{\pi}\sum_{i=1}^{2N_2+1} w_{2i}(r_j)G_{2(i)}+\sum_{i=1}^{2N_1+1} H_{21}(r_j,r_{0i})v_{1i}G_{1(i)}+\sum_{i=1}^{2N_2+1} H_{22}(r_j,r_{0i})v_{2i}G_{2(i)}+\sum_{i=1}^{2N_3+1} H_{23}(r_j,s_{0i})v_{3i}G_{3(i)} + \sum_{i=1}^{2N_3+1} H_{24}(r_j,s_{0i})v_{3i}^*G_{3(i)}^*=q_2(r_j),\quad j=1,\ldots,2N_2, \tag{38b}$$

$$\frac{R_3}{(1-s_j)^{\beta_3}(1+s_j)^{\alpha_3}}\sum_{m=1}^{3} B_mG_{3(I+m)}+\frac{P_3}{\pi}\sum_{i=1}^{2N_3+1} w_{3i}(s_j)G_{3(i)}+\sum_{i=1}^{2N_1+1} H_{31}(s_j,r_{0i})v_{1i}G_{1(i)}+\sum_{i=1}^{2N_2+1} H_{32}(s_j,r_{0i})v_{2i}G_{2(i)} + \sum_{i=1}^{2N_3+1} H_{33}(s_j,s_{0i})v_{3i}G_{3(i)}+\sum_{i=1}^{2N_3+1} H_{34}(s_j,s_{0i})v_{3i}^*G_{3(i)}^*=q_3(s_j),\quad j=1,\ldots,2N_3 \tag{38c}$$

subject to, in the case of an internal crack,

$$\sum_{i=1}^{2N_1+1} v_{1i}G_{1(i)}=0, \tag{39a}$$

$$\sum_{i=1}^{2N_2+1} v_{2i}G_{2(i)}=0 \tag{39b}$$

or, in the case of an edge crack,

$$h_{11}(\beta)G_{1(1)}+h_{12}(\beta)G_{2(1)}+h_{13}(\beta)G_{3(2N_3+1)}+h_{14}(\beta)G_{3(2N_3+1)}^*=0, \tag{40a}$$

$$h_{21}(\beta)G_{1(1)} + h_{22}(\beta)G_{2(1)} + h_{23}(\beta)G_{3(2N_3+1)} + h_{24}(\beta)G^*_{3(2N_3+1)} = 0, \tag{40b}$$

$$h_{31}(\beta)G_{1(1)} + h_{32}(\beta)G_{2(1)} + h_{33}(\beta)G_{3(2N_3+1)} + h_{34}(\beta)G^*_{3(2N_3+1)} = 0 \tag{40c}$$

and

$$\sum_{i=1}^{2N_3+1} v_{3i}G_{3(i)} - v^*_{3i}G^*_{3(i)} = 0, \tag{41a}$$

$$\sum_{i=1}^{2N_3+1} v_{3i}G_{3(i)} + v^*_{3i}G^*_{3(i)} = 0, \tag{41b}$$

$$\sum_{i=1}^{2N_3+1} [s_{0i} - 1][v_{3i}G_{3(i)} + v^*_{3i}G^*_{3(i)}] = 0 \tag{41c}$$

in which $I = j - 1$ or $j - 2$ for odd and even values of j, respectively, and N_i indicates the number of integration intervals. The typographical error-free form of the singular weight functions, $w_i(r_j)$, $w_i(s_j)$, and v_i, and the Lagrange coefficients, B_m, are given by Kabir et al. (1998). Finally, the discrete form of the singular integral equations, Eq. (38), and constraint equations, Eqs. (39)–(41), can be cast into the form

$$A_{ji}G_i = q_j, \quad i = 1, 2, \ldots, N, \ j = 1, 2, \ldots, M. \tag{42}$$

In the case of an internal crack, the number of unknowns, G_i is equal to the number of equations, i.e, $N = M = 1 + \Sigma_{k=1}^{3} 2N_k + 1$, leading to a unique solution. However, in the case of an edge crack, the number of unknowns, G_i, is one less than the number of equations, i.e, $M = N + 1$, leading to an over-determined system of equations. Therefore, the system of equations is solved in the sense of least-squares minimization.

5. Numerical results

In the solution of the integral equations concerning both the internal and edge crack configurations, the number of subintervals associated with each unknown function is chosen as 200 in order to ensure their convergence. The parameter C_h, the measure of material orthotropy, is useful in characterizing the anisotropy of orthotropic materials and also crystals with other symmetries. However, it is very difficult to give a simple physical interpretation for C_h. Results are given for five different substrate materials. The properties of these materials and the corresponding values of C_h are shown in Table 1. Since $C_h = 0$ corresponds to an isotropic material, Material 3 may be considered as "almost" isotropic. The material of the cover plate is assumed to be isotropic with shear modulus $G = 5.9931 \times 10^9$ Pa and Poisson's ratio $\nu = 0.3$. These material properties for the substrate and the cover plate are the same as those given by Mahajan (1991).

Table 1
Stiffness properties for substrate materials

Material	$C_{11} \times 10^{11}$ Pa	$C_{12} \times 10^{10}$ Pa	$C_{22} \times 10^{11}$ Pa	$C_{66} \times 10^{10}$ Pa	C_h
1	1.0100	2.7430	0.3592	0.4905	6.8222
2	0.5966	0.6764	0.1712	0.5592	3.0358
3	0.2088	0.9012	0.2101	0.5971	−0.0022
4	1.6800	6.6000	1.6800	8.4000	−1.0944
5	1.1904	5.3840	1.1904	5.9520	−1.3137

The validity of the present analysis is examined by considering Material 3 for the substrate. For this case, the material properties of the plate and the substrate are close to each other. As shown in Fig. 2, the normalized stress intensity factors associated with the internal crack tips approach unity as the crack of fixed length specified by $\ell_0 = (d-c)/2a = 1$ moves away from the boundary, recovering the solution for an infinite isotropic plate with an internal crack. Also, for $c \to 0$, the normalized stress intensity factor of $k_1(d)/(2^{\beta}\sigma_0\sqrt{d/2}) = 1.121$ is recovered for an edge crack in an isotropic half-space. Material 1, with the highest degree of material orthotropy, is considered in order to capture the effect of material orthotropy on the stress intensity factors.

Internal crack: For the case of an internal crack, the normalized stress intensity factors at the crack tips and at the corners of the plate are given in Tables 2 and 3 for a fixed normalized crack length, $\ell_0 = (d-c)/2a = 1$, and plate thickness-to-length ratios of $h/a = 3$, 5 and 7 while varying its distance from the boundary. The parameter $s_0 = (d+c)/2a$ indicates the distance from the boundary to the center of the crack. The results confirm the expected trend that the stress intensity factors at the crack tips increase with decreasing cover plate thickness and decreasing crack distance from the substrate boundary. A similar observation is also valid for the stress intensity factors at the corner of the plate aligned with the crack. Note that the shearing (mode II) stress intensity factors are small in comparison with the opening (mode I) values. This leads to the conclusion that sub-critical crack growth will be predominantly under mode I conditions. In Tables 4 and 5, the crack distance from the boundary, $s_0 = (d+c)/2a = 1$, is fixed and the normalized crack length denoted by the parameter $l_0 = (d-c)/2a$ is varied for plate thickness-to-length ratios of $h/a = 3$, 5 and 7. As expected, the stress intensity factors at the crack tips increase with increasing crack length.

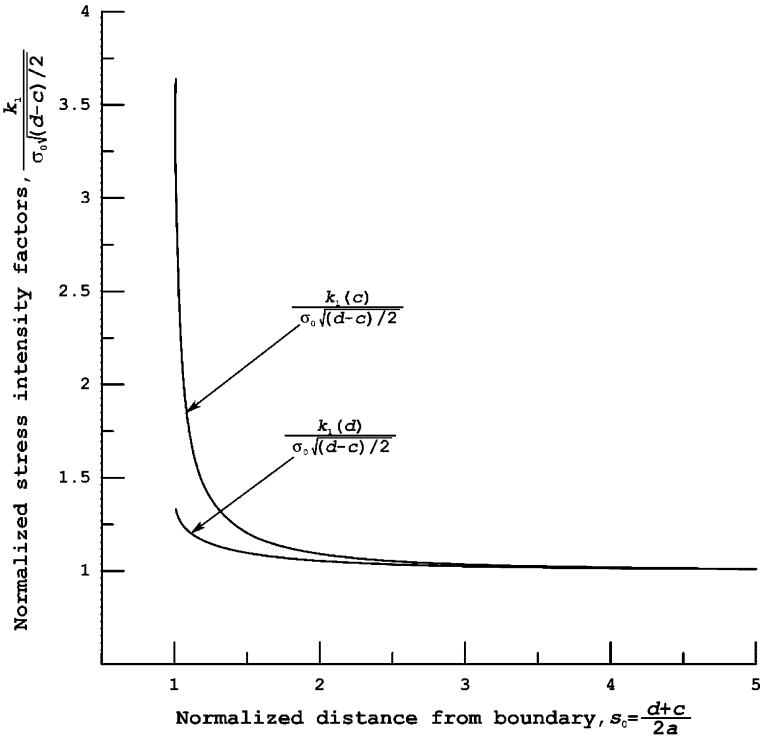

Fig. 2. Normalized stress intensity factors for an internal crack in an "almost" isotropic substrate (Material 3) for varying crack depth from the boundary.

Table 2
Normalized stress intensity factors at the internal crack tips for varying crack distance from boundary and for various plate thicknesses (Material 1, $\ell_0 = (d-c)/2a = 1$)

$s_0 = \frac{d+c}{2a}$	$\frac{k_1(c)}{\sigma_0\sqrt{(d-c)/2}}$	$\frac{k_1(d)}{\sigma_0\sqrt{(d-c)/2}}$	$\frac{k_2(c)}{\sigma_0\sqrt{(d-c)/2}}$	$\frac{k_2(d)}{\sigma_0\sqrt{(d-c)/2}}$
$a/h = 3$				
1.01	3.010	1.208	0.292	−0.066
1.05	1.814	1.154	0.056	−0.049
1.10	1.503	1.126	0.015	−0.040
1.50	1.109	1.055	−0.016	−0.018
2.00	1.047	1.031	−0.014	−0.011
3.00	1.018	1.014	−0.009	−0.006
5.00	1.007	1.006	−0.004	−0.003
$a/h = 5$				
1.01	3.016	1.218	0.191	−0.058
1.05	1.832	1.164	0.023	−0.040
1.10	1.522	1.134	−0.001	−0.031
1.50	1.119	1.059	−0.013	−0.012
2.00	1.051	1.033	−0.010	−0.008
3.00	1.020	1.015	−0.006	−0.004
5.00	1.007	1.006	−0.003	−0.002
$a/h = 7$				
1.01	3.022	1.225	0.129	−0.051
1.05	1.844	1.171	0.004	−0.034
1.10	1.535	1.140	−0.008	−0.025
1.50	1.126	1.061	−0.010	−0.009
2.00	1.054	1.034	−0.008	−0.006
3.00	1.021	1.015	−0.005	−0.003
5.00	1.007	1.006	−0.002	−0.001

Edge crack: In the presence of an edge crack, the strength of the singularity, β (Eq. (14c)) is obtained from the asymptotic analysis for the junction of a plate corner and edge crack surface in the substrate. The parameter, β is not dependent on the plate material properties but the half-space material properties. Its variation which does not appear to have a functional relationship is presented in Table 6 for materials 1–5 with varying degree of orthotropy controlled by the dimensionless anisotropy parameter, C_h. The normalized stress intensity factors at the tip of an edge crack and at the corners of the plate for varying normalized crack length d/a and plate thickness-to-length ratios of $h/a = 3$, 5 and 7 are presented in Tables 7 and 8, respectively. The stress intensity factors at the crack tip for both modes I and II increase as the crack tip approaches the boundary. As shown in Fig. 3, the stress intensity factors for all three plate thicknesses reach the limiting value of 1.297 for the opening mode as the crack length becomes larger than the length of the plate. As presented in Table 7, the stress intensity factors for the shearing mode decrease for increasing crack length. The normalized stress intensity factors at the junction of the plate and crack surface are small in comparison with the values at the other edge of the plate. As the crack tip approaches the boundary, the stress intensity factors of both modes associated with the corners of the plate increase. The comparison of the results in Table 7(materials 1 and 3), reveals the effect of material orthotropy on the stress intensity factors for an edge crack. The results in these tables also capture the effect of reinforcement on the stress intensity factors. As expected, the effect of the reinforcement on the stress intensity factors diminishes as the crack tip moves away from the boundary. In Table 7, as the crack tip moves away from the boundary, the normalization of the limiting value of $(k_1(d)/(\sigma_0\sqrt{d/2}) = 1.370)/2^\beta$ with $\beta = 0.28937205$ yields the well-known result of 1.121 for an edge crack in an isotropic half-space.

Table 3
Normalized stress intensity factors at the plate corners in the presence of an internal crack for varying crack distance from boundary and for various plate thicknesses (Material 1, $\ell_0 = (d-c)/2a = 1$)

$s_0 = \frac{d+c}{2a}$	$\frac{\eta k_1(-2a) + \mathrm{i}k_2(-2a)}{\sigma_0 a^{\alpha_3}}$	$\frac{\eta k_1(0) + \mathrm{i}k_2(0)}{\sigma_0 a^{\beta_3}}$
$a/h = 3$		
1.05	$0.180 - 0.093\mathrm{i}$	$0.831 + 0.390\mathrm{i}$
1.10	$0.197 - 0.101\mathrm{i}$	$0.570 + 0.270\mathrm{i}$
1.50	$0.231 - 0.123\mathrm{i}$	$0.241 + 0.140\mathrm{i}$
2.00	$0.220 - 0.123\mathrm{i}$	$0.190 + 0.117\mathrm{i}$
3.00	$0.197 - 0.114\mathrm{i}$	$0.173 + 0.106\mathrm{i}$
5.00	$0.180 - 0.106\mathrm{i}$	$0.169 + 0.102\mathrm{i}$
$a/h = 5$		
1.05	$0.137 - 0.069\mathrm{i}$	$0.699 + 0.311\mathrm{i}$
1.10	$0.151 - 0.076\mathrm{i}$	$0.459 + 0.213\mathrm{i}$
1.50	$0.186 - 0.094\mathrm{i}$	$0.185 + 0.107\mathrm{i}$
2.00	$0.182 - 0.095\mathrm{i}$	$0.153 + 0.090\mathrm{i}$
3.00	$0.166 - 0.088\mathrm{i}$	$0.145 + 0.081\mathrm{i}$
5.00	$0.153 - 0.082\mathrm{i}$	$0.144 + 0.079\mathrm{i}$
$a/h = 7$		
1.05	$0.114 - 0.056\mathrm{i}$	$0.605 + 0.266\mathrm{i}$
1.10	$0.126 - 0.062\mathrm{i}$	$0.382 + 0.180\mathrm{i}$
1.50	$0.159 - 0.078\mathrm{i}$	$0.151 + 0.089\mathrm{i}$
2.00	$0.158 - 0.079\mathrm{i}$	$0.130 + 0.074\mathrm{i}$
3.00	$0.145 - 0.073\mathrm{i}$	$0.126 + 0.067\mathrm{i}$
5.00	$0.134 - 0.068\mathrm{i}$	$0.126 + 0.065\mathrm{i}$

Table 4
Normalized stress intensity factors at the internal crack tips for varying crack length and plate thickness (Material 1, $s_0 = (d+c)/2a = 1$)

$l_0 = \frac{d-c}{2a}$	$\frac{k_1(c)}{\sigma_0\sqrt{(d-c)/2}}$	$\frac{k_1(d)}{\sigma_0\sqrt{(d-c)/2}}$	$\frac{k_2(c)}{\sigma_0\sqrt{(d-c)/2}}$	$\frac{k_2(d)}{\sigma_0\sqrt{(d-c)/2}}$
$a/h = 3$				
0.10	0.980	0.983	−0.010	−0.011
0.25	0.987	0.991	−0.010	−0.012
0.50	1.028	1.017	−0.010	−0.015
0.75	1.164	1.064	−0.005	−0.024
0.90	1.464	1.118	0.018	−0.039
$a/h = 5$				
0.10	0.986	0.987	−0.008	−0.008
0.25	0.994	0.996	−0.008	−0.009
0.50	1.037	1.022	−0.009	−0.011
0.75	1.178	1.072	−0.008	−0.018
0.90	1.481	1.127	0.002	−0.031
$a/h = 7$				
0.10	0.989	0.990	−0.006	−0.007
0.25	0.998	0.999	−0.007	−0.007
0.50	1.043	1.026	−0.007	−0.009
0.75	1.188	1.076	−0.009	−0.015
0.90	1.493	1.133	−0.006	−0.025

Table 5
Normalized stress intensity factors at the plate corners in the presence of an internal crack for varying crack length and plate thickness (Material 1, $s_0 = (d + c)/2a = 1$)

$l_0 = \frac{d-c}{2a}$	$\frac{\eta k_1(-2a) + \mathrm{i}k_2(-2a)}{\sigma_0 a^{\alpha_3}}$	$\frac{\eta k_1(0) + \mathrm{i}k_2(0)}{\sigma_0 a^{\beta_3}}$
$a/h = 3$		
0.10	$0.171 - 0.101\mathrm{i}$	$0.171 + 0.101\mathrm{i}$
0.25	$0.175 - 0.102\mathrm{i}$	$0.177 + 0.104\mathrm{i}$
0.50	$0.186 - 0.105\mathrm{i}$	$0.206 + 0.117\mathrm{i}$
0.75	$0.195 - 0.104\mathrm{i}$	$0.304 + 0.157\mathrm{i}$
0.90	$0.186 - 0.097\mathrm{i}$	$0.538 + 0.253\mathrm{i}$
$a/h = 5$		
0.10	$0.145 - 0.078\mathrm{i}$	$0.145 + 0.078\mathrm{i}$
0.25	$0.147 - 0.079\mathrm{i}$	$0.149 + 0.080\mathrm{i}$
0.50	$0.154 - 0.081\mathrm{i}$	$0.166 + 0.091\mathrm{i}$
0.75	$0.156 - 0.080\mathrm{i}$	$0.237 + 0.123\mathrm{i}$
0.90	$0.145 - 0.073\mathrm{i}$	$0.435 + 0.200\mathrm{i}$
$a/h = 7$		
0.10	$0.127 - 0.065\mathrm{i}$	$0.127 + 0.065\mathrm{i}$
0.25	$0.129 - 0.065\mathrm{i}$	$0.129 + 0.067\mathrm{i}$
0.50	$0.133 - 0.067\mathrm{i}$	$0.140 + 0.075\mathrm{i}$
0.75	$0.132 - 0.065\mathrm{i}$	$0.192 + 0.103\mathrm{i}$
0.90	$0.121 - 0.060\mathrm{i}$	$0.363 + 0.169\mathrm{i}$

Table 6
Strength of singularity for the junction of the plate corner and an edge crack surface of the substrate for Materials 1–5

Material	β
1	0.28309954
2	0.20241910
3	0.28937205
4	0.27884158
5	0.29999538

Table 7
Normalized stress intensity factors at the tip of an edge crack for varying crack length and plate thickness (Materials 1 and 3)

d/a	$\frac{k_1(d)}{\sigma_0\sqrt{d/2}}$			$\frac{k_2(d)}{\sigma_0\sqrt{d/2}}$		
	$a/h = 3$	$a/h = 5$	$a/h = 7$	$a/h = 3$	$a/h = 5$	$a/h = 7$
Material 1						
0.10	1.553	1.499	1.460	0.102	0.074	0.057
0.20	1.407	1.384	1.367	0.047	0.034	0.026
0.50	1.315	1.312	1.309	0.008	0.007	0.006
1.00	1.298	1.298	1.298	−0.002	0.000	0.000
1.50	1.297	1.297	1.297	−0.003	−0.001	−0.001
Material 3						
0.10	1.773	1.700	1.643	0.164	0.128	0.102
0.20	1.553	1.521	1.495	0.082	0.065	0.052
0.50	1.405	1.401	1.396	0.018	0.016	0.014
1.00	1.373	1.373	1.373	−0.001	0.000	0.001
1.50	1.370	1.370	1.370	−0.002	−0.001	−0.001

Table 8
Normalized stress intensity factors at the plate corners for varying edge crack length and plate thickness (Material 1)

d/a	$\frac{\eta k_1(-2a)+ik_2(-2a)}{\sigma_0 a^{\alpha_3}}$	$\frac{\eta k_1(0)+ik_2(0)}{\sigma_0 a^{\beta}}$
$a/h=3$		
0.10	$0.137-0.089i$	$0.082-0.023i$
0.20	$0.127-0.085i$	$0.054-0.015i$
0.50	$0.091-0.068i$	$0.018-0.005i$
1.00	$0.040-0.040i$	$-0.502+0.014i$
1.50	$0.009-0.021i$	$-0.160+0.045i$
$a/h=5$		
0.10	$0.118-0.070i$	$0.082-0.023i$
0.20	$0.112-0.067i$	$0.049-0.014i$
0.50	$0.086-0.054i$	$0.005-0.002i$
1.00	$0.044-0.032i$	$-0.073+0.020i$
1.50	$0.017-0.017i$	$-0.208+0.058i$
$a/h=7$		
0.10	$0.104-0.059i$	$0.080-0.022i$
0.20	$0.100-0.056i$	$0.042-0.012i$
0.50	$0.078-0.046i$	$-0.004+0.001i$
1.00	$0.043-0.028i$	$-0.089+0.025i$
1.50	$0.019-0.015i$	$-0.247+0.068i$

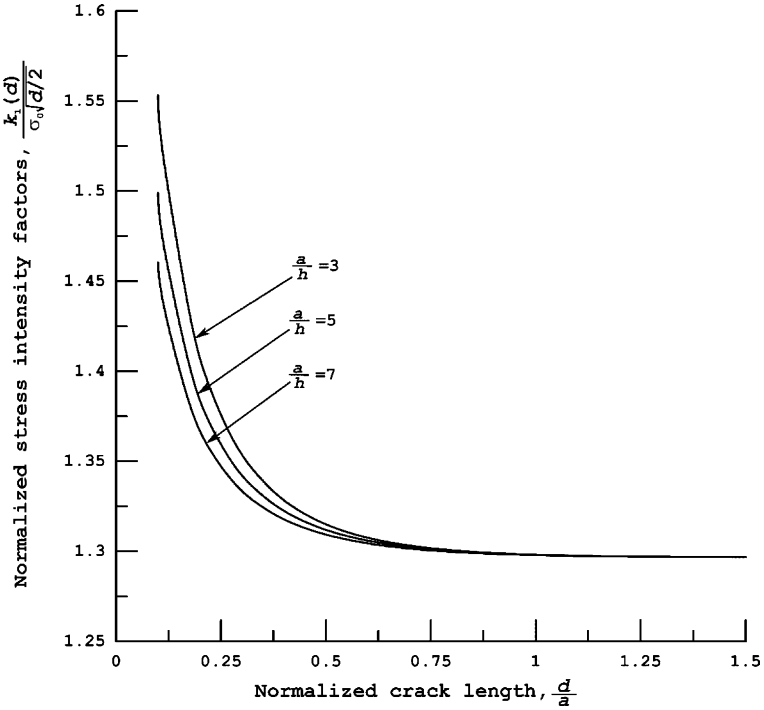

Fig. 3. Normalized stress intensity factors for an edge crack in an orthotropic substrate (Material 1) for varying crack length for a range of plate thickness-to-length ratios.

6. Conclusions

By solving the coupled singular integral equations with either a simple Cauchy kernel or with a generalized Cauchy kernel, this study investigated the effect of a reinforcement plate on the stress intensity factors of either an internal crack or an edge crack in an orthotropic substrate under uniform loading. The analysis revealed that the stress intensity factors at the internal crack tips increase with decreasing cover plate thickness and that they also increase with decreasing crack distance from the substrate boundary. Also, the normalized stress intensity factors at the crack tips increase with increasing crack length. The stress intensity factors at the tip of an edge crack and at the corners of the plate for both modes I and II increase as the crack tip approaches the boundary. The stress intensity factors of both modes associated with the corners of the plate also increase as the crack tip approaches the boundary. This study permits the investigation of the influence of material orthotropy on the stress intensification or the energy release rate to predict cracking and its direction.

Appendix A

The Green's functions, K_{ij} and M_{ij}, in Eqs. (1) and (2) due to a pair of dislocations at point (x_1, y_1) and concentrated forces at $(0, y_0)$ in the half-plane were derived by Pande and Chou (1971) and Wu and Chou (1982), respectively, as

$$K_{11}(x,y,x_1,y_1) = \frac{K_n\lambda^2}{2\pi}\left\{\frac{x-x_1}{\chi_1}[(x-x_1)^2-\lambda^2(y-y_1)^2]-\frac{x+x_1}{\chi_2}[(x+x_1)^2-\lambda^2(y-y_1)^2]\right\} + \frac{K_n\lambda^2}{\pi C_h}\left\{\frac{x+x_1}{\chi_2}[2\zeta+C_h(x+x_1)^2]\right\}-\frac{1}{\chi_3}[2(x+x_1)\zeta+C_h\{C_hx_1x^2+x(x+x_1)(x+3x_1) + x_1\lambda^2(y-y_1)^2\}],$$

$$K_{12}(x,y,x_1,y_1) = -\frac{K_e\lambda^2}{2\pi}\left\{\frac{y-y_1}{\chi_1}[(C_h+3)(x-x_1)^2+\lambda^2(y-y_1)^2]-\frac{y-y_1}{\chi_2}[(C_h+3)(x+x_1)^2 + \lambda^2(y-y_1)^2]\right\}+\frac{K_e\lambda^2}{\pi C_h}\left\{\frac{y-y_1}{\chi_2}[2\zeta+C_h(x+x_1)^2]-\frac{y-y_1}{\chi_3}[2\zeta+C_h(x^2+x_1^2)]\right\},$$

$$K_{21}(x,y,x_1,y_1) = \frac{K_n\lambda^2}{2\pi}\left\{\frac{y-y_1}{\chi_1}[(x-x_1)^2-\lambda^2(y-y_1)^2]-\frac{y-y_1}{\chi_2}[(x+x_1)^2-\lambda^2(y-y_1)^2]\right\} + \frac{K_n\lambda^2}{\pi C_h}\left\{\frac{y-y_1}{\chi_2}[2\zeta+C_h(x+x_1)^2]-\frac{y-y_1}{\chi_3}[2\zeta+C_h(x^2+x_1^2)]\right\},$$

$$K_{22}(x,y,x_1,y_1) = \frac{K_e}{2\pi}\left\{\frac{x-x_1}{\chi_1}[(x-x_1)^2-\lambda^2(y-y_1)^2]-\frac{x+x_1}{\chi_2}[(x+x_1)^2-\lambda^2(y-y_1)^2]\right\} - \frac{K_e}{\pi C_h}\left\{\frac{x+x_1}{\chi_2}[2\zeta+C_h\lambda^2(y-y_1)^2]-\frac{1}{\chi_3}[2(x+x_1)\zeta+C_h\{C_hxx_1^2+x_1(x+x_1)(3x+x_1) + x\lambda^2(y-y_1)^2\}]\right\},$$

$$K_{31}(x,y,x_1,y_1)=\frac{K_n}{2\pi}\left\{\frac{x-x_1}{\chi_1}[(x-x_1)^2+(C_h+3)\lambda^2(y-y_1)^2]-\frac{x+x_1}{\chi_2}[(x+x_1)^2+(C_h+3)\lambda^2(y-y_1)^2]\right\}-\frac{K_n}{\pi C_h}\left\{\frac{x+x_1}{\chi_2}[2\zeta+C_h\lambda^2(y-y_1)^2]-\frac{1}{\chi_3}[2(x+x_1)\zeta+C_h\{C_hxx_1^2+x_1(x+x_1)(3x+x_1)+x\lambda^2(y-y_1)^2\}]\right\},$$

$$K_{32}(x,y,x_1,y_1)=\frac{K_e}{2\pi}\left\{\frac{y-y_1}{\chi_1}[(x-x_1)^2-\lambda^2(y-y_1)^2]-\frac{y-y_1}{\chi_2}[(x+x_1)^2-\lambda^2(y-y_1)^2]\right\}-\frac{K_e}{\pi C_h}\left\{\frac{y-y_1}{\chi_2}[2\zeta+C_h\lambda^2(y-y_1)^2]-\frac{y-y_1}{\chi_3}[2\zeta+C_h\{(C_h+4)x_1^2+2x_1x+\lambda^2(y-y_1)^2\}]\right\},$$

$$K_{13}(x,y,y_0)=-\frac{\lambda^3x^2(y-y_0)\sqrt{C_h+4}}{\pi\{x^4+\lambda^2(C_h+2)x^2(y-y_0)^2+\lambda^4(y-y_0)^4\}},$$

$$K_{14}(x,y,y_0)=-\frac{\lambda x^3\sqrt{C_h+4}}{\pi\{x^4+\lambda^2(C_h+2)x^2(y-y_0)^2+\lambda^4(y-y_0)^4\}},$$

$$K_{23}(x,y,y_0)=-\frac{\lambda^3x(y-y_0)^2\sqrt{C_h+4}}{\pi\{x^4+\lambda^2(C_h+2)x^2(y-y_0)^2+\lambda^4(y-y_0)^4\}},$$

$$K_{24}(x,y,y_0)=-\frac{\lambda x^2(y-y_0)\sqrt{C_h+4}}{\pi\{x^4+\lambda^2(C_h+2)x^2(y-y_0)^2+\lambda^4(y-y_0)^4\}},$$

$$K_{33}(x,y,y_0)=-\frac{\lambda^3(y-y_0)^3\sqrt{C_h+4}}{\pi\{x^4+\lambda^2(C_h+2)x^2(y-y_0)^2+\lambda^4(y-y_0)^4\}},$$

$$K_{34}(x,y,y_0)=-\frac{\lambda x(y-y_0)^2\sqrt{C_h+4}}{\pi\{x^4+\lambda^2(C_h+2)x^2(y-y_0)^2+\lambda^4(y-y_0)^4\}},$$

$$M_{11}(0,y,x_1,y_1)=\frac{\lambda x_1^2(y-y_1)\sqrt{C_h+4}}{\pi\{[x_1^2+\lambda^2(y-y_1)^2]^2+C_hx_1^2\lambda^2(y-y_1)^2\}},$$

$$M_{12}(0,y,x_1,y_1)=-\frac{\lambda x_1^3\sqrt{C_h+4}}{\pi\{[x_1^2+\lambda^2(y-y_1)^2]^2+C_hx_1^2\lambda^2(y-y_1)^2\}},$$

$$M_{21}(0,y,x_1,y_1)=-\frac{\lambda^3x_1(y-y_1)^2\sqrt{C_h+4}}{\pi\{[x_1^2+\lambda^2(y-y_1)^2]^2+C_hx_1^2\lambda^2(y-y_1)^2\}},$$

$$M_{22}(0,y,x_1,y_1)=\frac{\lambda^3x_1^2(y-y_1)\sqrt{C_h+4}}{\pi\{[x_1^2+\lambda^2(y-y_1)^2]^2+C_hx_1^2\lambda^2(y-y_1)^2\}},$$

$$M_{13}(y,y_0) = -R_1\delta(y-y_0),$$

$$M_{14}(y,y_0) = -R_2\frac{1}{\pi(y-y_0)},$$

$$M_{23}(y,y_0) = -S_2\frac{1}{\pi(y-y_0)},$$

$$M_{24}(y,y_0) = S_1\delta(y-y_0),$$

where

$$K_e = (\overline{C}_{12}+C_{12})\sqrt{\frac{C_{66}(\overline{C}_{12}-C_{12})}{C_{22}(\overline{C}_{12}+C_{12}+2C_{66})}}, \quad \text{with } \overline{C}_{12} = \sqrt{C_{11}C_{22}},$$

$$K_n = \frac{K_e}{\lambda^2}, \quad \text{with } \lambda = \left(\frac{C_{11}}{C_{12}}\right)^{1/4},$$

$$\zeta = (x+x_1)^2 + \lambda^2(y-y_1)^2,$$

$$\chi_1 = \{(x-x_1)^2 + \lambda^2(y-y_1)^2\}^2 + C_h(x-x_1)^2\lambda^2(y-y_1)^2,$$

$$\chi_2 = \zeta^2 + C_h(x+x_1)^2\lambda^2(y-y_1)^2,$$

$$\chi_3 = (\zeta + C_h x_1 x)^2 + C_h(x-x_1)^2\lambda^2(y-y_1)^2,$$

$$C_h = \frac{(\overline{C}_{12}+C_{12})(\overline{C}_{12}-C_{12}-2C_{66})}{\overline{C}_{12}C_{66}},$$

$$S_1 = \frac{Q_2}{P_1Q_2+P_2Q_1}, \qquad S_2 = \frac{Q_1}{P_1Q_2+P_2Q_1},$$

$$R_1 = -\frac{P_1}{P_1Q_2+P_2Q_1}, \qquad R_2 = \frac{P_2}{P_1Q_2+P_2Q_1},$$

$$P_1 = C_{12} + \frac{s_2-s_1}{d_2-d_1}C_{11}, \qquad P_2 = \frac{s_2d_2-s_1d_1}{d_2-d_1}C_{66},$$

$$Q_1 = \frac{s_1d_2-s_2d_1}{d_2-d_1}C_{11}, \qquad Q_2 = C_{66}\left\{1+\frac{d_1d_2(s_2-s_1)}{d_2-d_1}\right\},$$

$$d_1 = \frac{1-\beta_1 s_1^2}{\beta_3 s_1}, \qquad d_2 = \frac{1-\beta_1 s_2^2}{\beta_3 s_2},$$

$$\beta_1 = \frac{C_{11}}{C_{66}}, \quad \beta_2 = \frac{C_{22}}{C_{66}}, \quad \beta_3 = 1+\frac{C_{12}}{C_{66}}, \quad \beta_4 = \frac{\beta_3^2-\beta_1\beta_2-1}{\beta_1}, \quad \beta_5 = \frac{\beta_2}{\beta_1}.$$

The parameters s_1 and s_2 ($\mathrm{Re}(s_1, s_2) > 0$) are the roots of the characteristic equation

$$s^4 + \beta_4 s^2 + \beta_5 = 0.$$

Regardless of the nature of the roots s_1 and s_2, the constants P_1, P_2, Q_1, and Q_2 are always real. Also, it can be shown that $R_1 = S_1$ for all orthotropic materials.

The kernels of the singular integral equations given by Eqs. (9a), (9b), and (10) are defined as

$$N_{11}(x,t) = \frac{2}{\pi C_h}\left\{\frac{C_h+4}{2(x+t)} - \frac{2x + t(C_h+2)}{x^2 + (C_h+2)xt + t^2}\right\},$$

$$N_{12}(x,t) = 0,$$

$$N_{13}(x,y_0) = \frac{\sqrt[2]{C_h+4}\,\lambda^3 y_0^3}{\pi K_n\{x^4 + \lambda^2(C_h+2)x^2y_0^2 + \lambda^4 y_0^4\}},$$

$$N_{14}(x,y_0) = -\frac{\sqrt[2]{C_h+4}\,\lambda x y_0^2}{\pi K_n\{x^4 + \lambda^2(C_h+2)x^2y_0^2 + \lambda^4 y_0^4\}},$$

$$N_{21}(x,t) = 0,$$

$$N_{22}(x,t) = \frac{2}{\pi C_h}\left\{\frac{Ch+4}{2(x+t)} - \frac{2x + t(C_h+2)}{x^2 + (C_h+2)xt + t^2}\right\},$$

$$N_{23}(x,y_0) = -\frac{\sqrt[2]{C_h+4}\,\lambda^3 x y_0^2}{\pi K_e\{x^4 + \lambda^2(C_h+2)x^2y_0^2 + \lambda^4 y_0^4\}},$$

$$N_{24}(x,y_0) = \frac{\sqrt[2]{C_h+4}\,\lambda y_0 x^2}{\pi K_e\{x^4 + \lambda^2(C_h+2)x^2y_0^2 + \lambda^4 y_0^4\}},$$

$$N_{31}(y,t) = \frac{\beta_{22}K_n(C_h+4)t\lambda^2 y^2}{\pi S_2\{(t^2+\lambda^2y^2)^2 + C_h\lambda^2y^2t^2\}},$$

$$N_{32}(y,t) = -\frac{\beta_{22}K_e(C_h+4)t^2 y}{\pi S_2\{(t^2+\lambda^2y^2)^2 + C_h\lambda^2y^2t^2\}},$$

$$N_{33}(y,y_0) = -\frac{1}{S_2}\left\{C + \frac{Dh^2}{4}\right\}H(y-y_0),$$

$$N_{34}(y,y_0) = -\frac{Dh}{2S_2}(y-y_0)H(y-y_0),$$

$$N_{41}(y,t) = -\frac{\beta_{22}K_n(C_h+4)t^2 y}{\pi R_2\{(t^2+\lambda^2y^2)^2 + C_h\lambda^2y^2t^2\}},$$

$$N_{42}(y,t) = \frac{\beta_{22}K_e(C_h+4)t^3}{\pi\lambda^2 R_2\{(t^2+\lambda^2y^2)^2 + C_h\lambda^2y^2t^2\}},$$

$$N_{43}(y,y_0) = \frac{Dh}{2R_2}(y-y_0)H(y-y_0),$$

$$N_{44}(y,y_0) = -\frac{B}{R_2}H(y-y_0) + \frac{D}{2R_2}(y-y_0)^2 H(y-y_0).$$

The kernels M_j in Eq. (10) are defined in terms of N_{ij} as

$$M_1(y,t) = N_{31}(y,t) - \mathrm{i}\eta N_{41}(y,t),$$

$$M_2(y,t) = N_{32}(y,t) - \mathrm{i}\eta N_{42}(y,t),$$

$$M_3(y,y_0) = \frac{1}{2}\left[-\mathrm{i}N_{33}(y,y_0) - \eta N_{43}(y,y_0) + \frac{N_{34}(y,y_0)}{\eta} - \mathrm{i}N_{44}(y,y_0)\right],$$

$$M_4(y,y_0) = \frac{1}{2}\left[\mathrm{i}N_{33}(y,y_0) + \eta N_{43}(y,y_0) + \frac{N_{34}(y,y_0)}{\eta} - \mathrm{i}N_{44}(y,y_0)\right].$$

The parameters and the kernels in Eq. (30) are defined as

$$P_1 = \frac{2}{K_n}, \quad P_2 = \frac{2}{K_e}, \quad P_3 = -\mathrm{i}, \quad R_3 = -\gamma,$$

$$H_{11}(r,r_0) = \frac{d-c}{K_n}N_{11}(x,t), \quad H_{12}(r,r_0) = \frac{d-c}{K_e}N_{12}(x,t),$$

$$H_{13}(r,s_0) = \frac{a}{2}\left\{ -\mathrm{i}N_{13}(x,y_0) + \frac{1}{\eta}N_{14}(x,y_0)\right\}, \quad H_{14}(r,s_0) = \frac{a}{2}\left\{ iN_{13}(x,y_0) + \frac{1}{\eta}N_{14}(x,y_0)\right\},$$

$$H_{21}(r,r_0) = \frac{d-c}{K_n}N_{21}(x,t), \quad H_{22}(r,r_0) = \frac{d-c}{K_e}N_{22}(x,t),$$

$$H_{23}(r,s_0) = \frac{a}{2}\left\{ -\mathrm{i}N_{23}(x,y_0) + \frac{1}{\eta}N_{24}(x,y_0)\right\}, \quad H_{24}(r,s_0) = \frac{a}{2}\left\{ \mathrm{i}N_{23}(x,y_0) + \frac{1}{\eta}N_{24}(x,y_0)\right\},$$

$$H_{31}(s,r_0) = \frac{d-c}{K_n}M_1(y,t), \quad H_{32}(s,r_0) = \frac{d-c}{K_e}M_2(y,t),$$

$$H_{33}(s,s_0) = aM_3(y,y_0), \quad H_{34}(s,s_0) = aM_4(y,y_0).$$

Appendix B

From the equilibrium of a section of the plate subjected to surface tractions (shear and normal stresses along the interface between the plate and substrate) as shown in Fig. 4, the resultant membrane force, N_{yy}, transverse shear force, Q_{yy}, and resultant moment, M_{yy}, are expressed in the form

$$N_{yy}(y) = -\int_{-2a}^{y} f_3(y_0)\,\mathrm{d}y_0,$$

$$Q_{yy}(y) = \int_{-2a}^{y} f_4(y_0)\,\mathrm{d}y_0,$$

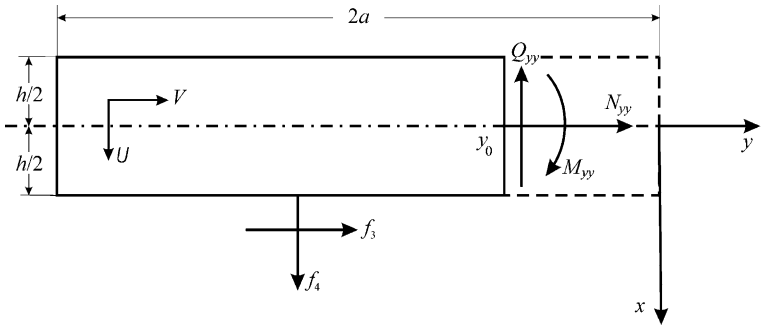

Fig. 4. Free-body diagram of the plate segment bonded to the substrate.

$$M_{yy}(y) = \frac{h}{2}\int_{-2a}^{y} f_3(y_0)\,\mathrm{d}y_0 + \int_{-2a}^{y}(y-y_0)f_4(y_0)\,\mathrm{d}y_0.$$

In the plate, the displacement component in the thickness direction is represented by $U = U_0(y)$ and, in the horizontal direction by $V = V_0(y) - x\psi_y(y)$, in which $\psi_y(y)$ denotes the rotation of the plate about the z-axis. The mid-plane displacement components are denoted by U_0 and V_0 in x and y directions, respectively. Based on these displacement representations, the strain components of interest may be expressed as

$$\varepsilon_{yy}(x,y) = \frac{\mathrm{d}}{\mathrm{d}y}V_0(y) - x\frac{\mathrm{d}}{\mathrm{d}y}\psi_y(y),$$

$$\gamma_{xy}(y) = \frac{\mathrm{d}}{\mathrm{d}y}U_0(y) - \psi_y(y).$$

Utilizing these kinematic relations in conjunction with Hooke's law under plane strain conditions while including the shear correction factor of 5/6 leads to

$$\frac{\mathrm{d}}{\mathrm{d}y}V\left(\frac{h}{2},y\right) = CN_{yy}(y) - \frac{h}{2}\frac{\mathrm{d}}{\mathrm{d}y}\psi_y(y),$$

$$\frac{\mathrm{d}}{\mathrm{d}y}\psi_y(y) = DM_{yy}(y),$$

$$\frac{\mathrm{d}}{\mathrm{d}y}U_0(y) = \psi_y(y) - BQ_{yy}(y)$$

in which the constants B, C, and D are defined in terms of engineering material constants as $B = 6/hG_{xy}$, $C = (1 - v_{yz}v_{zy})/hE_{yy}$, and $D = 12(1 - v_{yz}v_{zy})/h^3E_{yy}$.

Substitution of the resultant forces, N_{yy} and Q_{yy}, and moment, M_{yy}, in terms of the shear and normal stresses, $f_3(y)$ and $f_4(y)$, gives the displacement gradients along the interface between the plate and substrate as follows

$$\frac{\partial}{\partial y}U(y) = \psi_y(-2a) + \frac{Dh}{2}\int_{-2a}^{y}(y-y_0)f_3(y_0)\,\mathrm{d}y_0 + \frac{D}{2}\int_{-2a}^{y}(y-y_0)^2f_4(y_0)\,\mathrm{d}y_0 - B\int_{-2a}^{y}f_4(y_0)\,\mathrm{d}y_0,$$

$$\frac{\partial}{\partial y}V(h/2,y) = -\left(C + \frac{Dh^2}{4}\right)\int_{-2a}^{y} f_3(y_0)\,\mathrm{d}y_0 - \frac{Dh}{2}\int_{-2a}^{y}(y-y_0)f_4(y_0)\,\mathrm{d}y_0$$

in which $\psi_y(-2a)$ is an unknown constant representing the rotation at $x = -2a$.

Appendix C

As given by Muskhelishvili (1953), a sectionally holomorphic function defined by

$$F(z_i) = \frac{1}{\pi}\int_c^d \frac{f(t)}{t - z_i}\,\mathrm{d}t, \quad i = 1, 2,$$

with

$$f(t) = \frac{G(t)}{(d-t)^{\alpha}(t-c)^{\beta}}, \quad 0 < \mathrm{Re}(\alpha,\beta) < 1,\ c < t < d,\ G(c) \neq 0,\ G(d) \neq 0$$

has the following asymptotic expression near the end points c and d:

$$\frac{1}{\pi}\int_c^d \frac{f(t)}{t - z_1}\,\mathrm{d}t = \frac{G(c)}{(d-c)^{\alpha}}\frac{\mathrm{e}^{\mathrm{i}\pi\beta}}{\sin\pi\beta}\frac{1}{(z_1 - c)^{\beta}} + h(z_1),$$

$$\frac{1}{\pi}\int_c^d \frac{f(t)}{t - z_2}\,\mathrm{d}t = -\frac{G(d)}{(d-c)^{\beta}}\frac{1}{\sin\pi\alpha}\frac{1}{(z_2 - d)^{\alpha}} + s(z_2).$$

As sketched in Fig. 5, outside the cut defined by $[c, d]$, the complex variables, z_i, are expressed as

$$z_1 = c + r_1(x-c)\mathrm{e}^{\mathrm{i}\theta_1}, \quad 0 < \theta_1 < 2\pi,$$

$$z_2 = d + r_2(d-x)\mathrm{e}^{\mathrm{i}\theta_2}, \quad -\pi < \theta_2 < \pi.$$

After substituting for z_1 and z_2, and separating the principal parts, the asymptotic expressions become

$$\frac{1}{\pi}\int_c^d \frac{f(t)}{t - z_1}\,\mathrm{d}t = \frac{G(c)}{(d-c)^{\alpha}}\frac{\mathrm{e}^{\mathrm{i}(\pi-\theta_1)\beta}}{\sin\pi\beta}\frac{1}{r_1^{\beta}(x-c)^{\beta}} + h(x),$$

$$\frac{1}{\pi}\int_c^d \frac{f(t)}{t - z_2}\,\mathrm{d}t = -\frac{G(d)}{(d-c)^{\beta}}\frac{\mathrm{e}^{-\mathrm{i}\theta_2\alpha}}{\sin\pi\alpha}\frac{1}{r_2^{\beta}(d-x)^{\alpha}} + s(x),$$

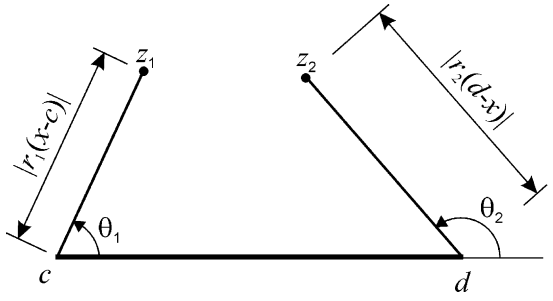

Fig. 5. Description of the points z_1 and z_2 in relation to the ends of cut.

where $h(x)$ and $s(x)$ are either bounded or have singularities that are a lower order than α and β. These asymptotic expressions are suitable for the behavior of singular integral equations with the generalized Cauchy kernels. Also derived by Muskhelishvili (1953), for the dominant part of the first singular integral equation, the asymptotic expression near the end points is expressed as

$$\frac{1}{\pi}\int_c^d \frac{f(t)}{t-x}\,\mathrm{d}t = \frac{G(c)}{(d-c)^{\alpha}}\frac{\cot\pi\beta}{(x-c)^{\beta}} - \frac{G(d)}{(d-c)^{\beta}}\frac{\cot\pi\alpha}{(d-x)^{\alpha}} + G_0(z), \quad c < x < d$$

in which $F_0(z)$ and $G_0(z)$ are either bounded or may have singularities that are a lower order than α and β.

References

Bogy, D.B., 1970. On the problem of edge-bonded elastic quarter-planes loaded at the boundary. International Journal of Solids and Structures 6, 1287–1313.

Delale, F., Erdogan, F., 1982. The crack problem for a half-plane stiffened by elastic cover plates. International Journal of Solids and Structures 18, 381–395.

Delale, F., Erdogan, F., Aydinoglu, M.N., 1981. Stresses in adhesively bonded joints: a closed form solution. Journal of Composite Materials 15, 249–271.

Erdogan, F., 1969. Approximate solution of systems of singular integral equations. SIAM Journal of Applied Mathematics 17, 1041–1059.

Erdogan, F., 1971. Analysis of elastic cover plates. Development in Mechanics Conference 6, 817–830.

Erdogan, F., Arin, K., 1972. A penny-shaped interface crack between an elastic layer and a half-space. International Journal of Engineering Science 10, 115–125.

Erdogan, F., Civelek, M.B., 1974. Contact problem for an elastic reinforcement bonded to an elastic plate. ASME Journal of Applied Mechanics 41, 1014–1018.

Erdogan, F., Gupta, G.D., 1971a. The problem of an elastic stiffener bonded to a half-plane. ASME Journal of Applied Mechanics 38, 937–942.

Erdogan, F., Gupta, G.D., 1971b. Layered composites with an interface flaw. International Journal of Solids and Structures 7, 1089–1107.

Erdogan, F., Gupta, G.D., 1972. On the numerical solution of singular integral equations. Quarterly of Applied Mathematics 30, 525–534.

Erdogan, F., Gupta, G.D., Cook, T.S., 1973. Numerical solution of singular integral equations. In: Sih, G.C. (Ed.), Methods of Analysis and Solutions of Crack Problems. Noordhoff International Publishing, Leyden, pp. 368–425.

Erdogan, F., Joseph, P.F., 1990. Mechanical modeling of multilayered films on an elastic substrate-part I: analysis, part II: results and discussion. Journal of Electronic Packaging 112, 309–326.

Goland, M., Reissner, E., 1944. The stress in cemented joints. ASME Journal of Applied Mechanics 11, A17–A27.

Goodier, J.N., Hsu, C.S., 1954. Transmission of tension from a bar to a plate. ASME Journal of Applied Mechanics 21, 147–150.

Hu, S.M., 1979. Film-edge-induced stress in substrates. Journal of Applied Physics 50, 4661–4666.

Hutchinson, J.W., Suo, Z., 1991. Mixed-mode cracking in layered materials. Advances in Applied Mechanics 29, 63–191.

Isomae, S., 1981. Stress distribution in silicon crystal substrates with thin films. Journal of Applied Physics 52, 2782–2791.

Isomae, S., 1985. Stress in silicon at Si_3N_4/SiO_2 film edges and viscoelastic behavior of SiO_2 films. Journal of Applied Physics 57, 216–223.

Kabir, H., Madenci, E., Ortega, A., 1998. Numerical solution of integral equations with logarithmic- Cauchy- and Hadamard-type singularities. International Journal for Numerical Methods in Engineering 41, 617–638.

Mahajan, R., 1991. Crack problems for an elastic film bonded to an orthotropic substrate. Ph.D. Dissertation, Lehigh University, Bethlehem, Pa.

Mahajan, R., Erdogan, F., Chou, Y.T., 1993. The crack problem for an orthotropic half-plane stiffened by elastic films. International Journal of Engineering Science 31, 403–424.

Miller, G.R., Keer, L.M., 1985. A numerical technique for the solution of singular integral equations of the second kind. Quarterly Journal of Applied Mathematics 43, 455–465.

Muki, R., Sternberg, E., 1968. On the stress analysis of overlapping bonded elastic sheets. International Journal of Solids and Structures 4, 75–94.

Muskhelishvili, I.N., 1953. Singular Integral Equations. Noordhoff N.V. Groningen, Holland.

Pande, C.S., Chou, Y.T., 1971. Edge dislocation in semi-infinite anisotropic media. Physica Status Solidi A 61, 499–504.
Quan, M.A., 1991. Analysis of a finite interface crack emitting from the junction of three sectors. Ph.D. Dissertation, University of California, Los Angeles.
Theocaris, P.S., Ioakimides, N., 1977. Numerical integration methods for the solution of singular integral equations. Quarterly of Applied Mathematics 32, 173–183.
Wu, R.S., Chou, Y.T., 1982. Line force in a two-phase orthotropic medium. ASME Journal of Applied Mechanics 49, 55–61.